Sensor systems

Exploiting Multimode Antennas for MIMO and AoA Estimation in Size-Constrained IoT Devices

Abel Zandamela[1*], Alessandro Chiumento[2], Nicola Marchetti[1**], Max J. Ammann[3***], and Adam Narbudowicz[1,4]

[1]CONNECT Centre, Trinity College Dublin, The University of Dublin, Dublin 2, Ireland
[2]Department of Pervasive Systems, University of Twente, 7522 NB Enschede, The Netherlands
[3]Antenna and High Frequency Research Centre, Technological University Dublin, Grangegorman, D07ADY7 Dublin, Ireland
[4]Department of Telecommunications and Teleinformatics, Wroclaw University of Science and Technology, 50-370 Wroclaw, Poland
*Member, IEEE
**Senior Member, IEEE
***Fellow, IEEE

Manuscript received 26 January 2023; accepted 10 February 2023. Date of publication 14 February 2023; date of current version 2 March 2023.

Abstract—This work proposes compact multimode Multiple-Input–Multiple-Output (MIMO) antennas for Angle of Arrival (AoA) estimation in miniaturized Internet of Things (IoT) systems. The method excites different orthogonal radiating modes (TM_{21}, TM_{02}, and TM_{31} modes) for beamforming capabilities, and the AoA performance is investigated using the Multiple Signal Classification (MUSIC) algorithm, executed using numerical and experimental data. The technique is tested at $2.238\,\text{GHz}$, while using an antenna diameter $< 7.5\,\text{cm}$. Overall, an envelope correlation coefficient < 0.01 is realized between all antenna ports, and a 360° field of view AoA estimation is demonstrated across the entire azimuthal plane with mean absolute errors smaller than 0.098°. Furthermore, it is shown that the capability of separating multiple simultaneous impinging signals is comparable to that of state-of-the-art circular arrays with similar number of RF transceivers, while offering, respectively, up to 35% and 71% antenna diameter and height miniaturization.

Index Terms—Sensor systems, Angle of Arrival (AoA) estimation, beamforming antennas, compact Internet of Things (IoT) systems, localization sensors, Multiple-Input–Multiple-Output (MIMO) antennas, Multiple Signal Classification (MUSIC) algorithm.

I. INTRODUCTION

With the advances of the Internet of Things (IoT) technology and ubiquitous connectivity, localization has become an indispensable feature of numerous cutting-edge technologies, such as smart cities, home automation, and connected healthcare systems [1]. Angle of Arrival (AoA) estimation is a popular localization method that offers reliable location measurements without the need for clock synchronization and allows for simultaneous detection of multiple impinging signals. However, it requires antenna arrays which are bulky structures with limited miniaturization capabilities. Moreover, AoA estimation is dependent on the number of array elements and the interspacing between them; in general, the larger the array aperture, the better the accuracy of the estimated angles [2], [3]. Furthermore, to simultaneously detect multiple impinging signals, one requires larger array structures, as to distinguish N different signals using state-of-the-art algorithms, one needs $N + 1$ antennas [3]. On the other hand, reducing the inter-element spacing in classical arrays is challenging, as it will cause increased mutual coupling and consequently decreased accuracy of localization.

Different techniques have been proposed for mitigation of mutual coupling effects in AoA estimation: direction-dependent analysis [4], machine-learning approach [5], mutual impedance method [6], phase center contour model [7], decoupling, and matching networks [8]. However, these solutions are either not discussed for closely spaced arrays, or the problem is not solved through antenna design novelty, often relying on the use of algorithms and calibration methods (resulting in additional computational time and antenna gain degradation), or the solutions have increased ohmic losses. Switched beams, single and multimode antennas have been investigated for AoA estimation, e.g., in [9], [10], [11], [12], [13], and [14]. Electronically steerable parasitic array radiators are used in [9]; leaky-wave antennas are reported in [10]; planar multimode antennas exploiting different sets of so called "characteristic modes" on the same antenna are studied in [13]; weight coefficients of the characteristic modes supported by a cubic structure are proposed in [14]. However, in the above works, size constraint is still an issue because parasitic elements require separation comparable to the element spacing in arrays to produce sufficient phase variations [9]; in addition, the switching between different antenna configurations, requires extra time for the AoA estimation, which can be a significant problem for multiple moving sources [9], [10]; matching networks are still required in [12]; accurate modeling techniques are needed for multiple impinging signals in [13]; or only single signal detection is analyzed [14].

This work proposes a new AoA estimation scheme using compact multimode Multiple-Input–Multiple-Output (MIMO) antennas; despite miniaturization, it offers better or comparable performance to state-of-the-art arrays with same number of RF transceivers, enabling localization in small IoT devices. The functionality is demonstrated using Multiple Signal Classification (MUSIC) algorithm [15] for easy comparison, albeit any state-of-the-art algorithm is also applicable and is expected to offer comparable advantages. The main contributions of this letter are as follows:

1) An AoA solution with 360° field of view (FoV) in the azimuth plane, which offers up to 35% size-reduction and 71% height miniaturization when compared to circular arrays. When

Corresponding author: Abel Zandamela (e-mail: zandamea@tcd.ie).
Associate Editor: F. Falcone.
Digital Object Identifier 10.1109/LSENS.2023.3244870

TABLE 1. Properties of the Excited Resonant Modes

Antenna Ports	Port 1 (TM_{21})	Port 2 (TM_{21})	Port 4 (TM_{31})	Port 5 (TM_{31})
E_z (V/m) 0° (500, 0, -500)	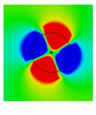	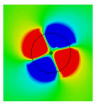	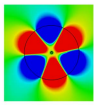	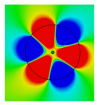
E_z (V/m) 90° (500, 0, -500)	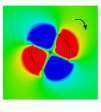	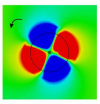	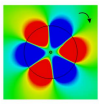	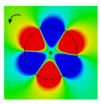
3D phase (deg) (360, 180, 0)				
3D Amplitude (1.75, -17.5, (dBi) -38.3)				

comparing with linear arrays, the solution offers 180° FoV and, respectively, 70% and 84% length and height miniaturization.

2) Due to the use of orthogonal radiating modes methodology, miniaturization is realized with good coupling characteristics.
3) Multiple impinging signals can be simultaneously localized with resolution comparable to that of the state-of-the-art systems, while keeping the miniaturization.

II. MULTIMODE MIMO ANTENNAS

The proposed multimode MIMO antennas incorporate collocated radiators that are fed using different ports, which facilitate excitation of distinct orthogonal radiating modes. Each mode has an omnidirectional radiation pattern and different angular phase distribution in the horizontal plane. The phase changes linearly to provide uniform performance; this is illustrated in Table 1, where the four phase varying modes used in this work are shown with respective electric fields. Note that larger number of modes and ports are also feasible.

All the excited modes have omnidirectional patterns in the azimuth plane (Table 1 fourth row). By exciting the ports with ±90° phase shift, the electric field rotates in opposite directions depending on phase polarity. By this principle, a clockwise direction is seen for ports 1 and 4, and counter-clockwise direction for ports 2 and 5 (see the E_z-components for 0° and 90° phase: Table 1 first and second rows). This ensures that the phase of the generated patterns changes in two opposing directions (see 3-D phase patterns: Table 1 third row). Compact IoT localization is enabled as the required phase difference for AoA estimation is obtained through phase-variation within radiating modes, and not via the distance between elements. Moreover, the proposed technique also ensures good coupling characteristics with miniaturization, due to the orthogonality between all the modes excited in the MIMO system.

A. Three-Port MIMO Antenna for 180° Field of View

The three-port MIMO antenna is shown in Fig. 1(a) and operates at the center frequency $f_0 = 2.238$ GHz. It consists of two dielectric-loaded circular patches separated by an RT5880 layer ($\epsilon_r = 2.2$ and $\tan\delta = 0.0009$) with height $h_2 = 0.79$ mm and diameter $D_{21} = 53.8$ mm. The top patch excites two orthogonal TM_{21} modes (Table 1 columns 2 and 3), while the bottom patch excites the

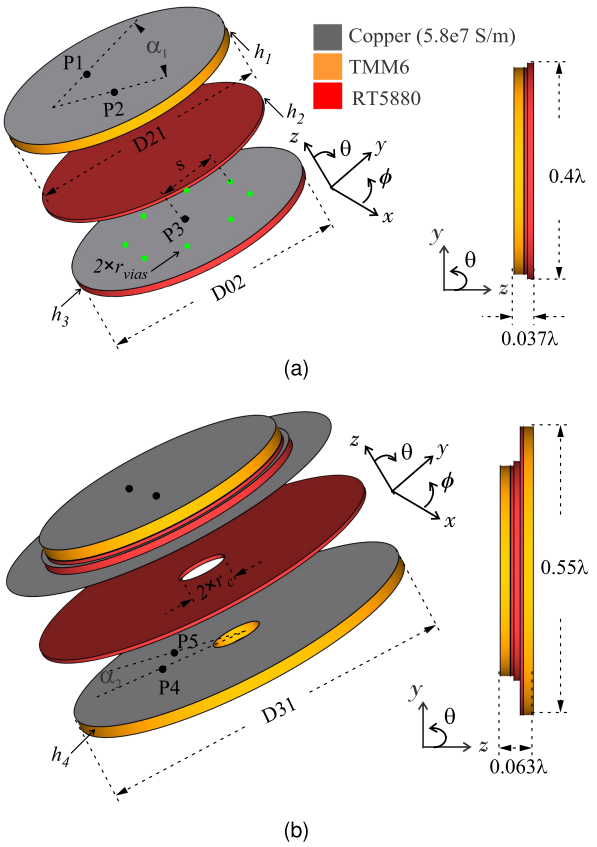

Fig. 1. Proposed multimode MIMO antennas (not drawn to scale). (a) Three-port MIMO design and (b) Five-port MIMO design.

monopole-like (TM_{02}) mode. The corresponding diameter for the specific TM_{nm} mode is approximated using the cavity mode analysis [16] as

$$D_{nm} = 2 \times R_{nm}, R_{nm} = \frac{\chi_{nm} c}{2\pi f_0 \sqrt{\epsilon_r}} \quad (1)$$

where c is the light velocity, and χ_{nm} is the mth zero of the derivative of the Bessel function, given as $\chi_{21} = 3.054$, $\chi_{02} = 3.831$, and $\chi_{31} = 4.201$.

The TM_{21} patch is supported by TMM6 substrate ($\epsilon_r = 6$ and $\tan\delta = 0.0023$), with height $h_1 = 2.54$ mm. From (1) $D_{21} = 53.2$ mm, and this value is then optimized, using finite element method full-wave simulations, to $D_{21} = 53.8$ mm. The feed positions P1 and P2 are located 9.5 mm from the disc center and rotated by $\alpha_1 = 225°$. The bottom patch is fed by P3, and uses RT5880 substrate with thickness $h_3 = 1.58$ mm and diameter $D_{02} = 54.8$ mm. The patch is shorted to its ground using eight vias of radius $r_{vias} = 0.25$ mm, located at $s = 13$ mm from the disk center and rotated by 45°. The vias allow for good isolation and frequency adjustment by controlling the value s. The final dimensions of the antenna are: 54.8 mm × 54.8 mm × 5.05 mm, corresponding to 0.4λ × 0.4λ × 0.037λ (where λ is the wavelength at f_0).

B. Five-Port MIMO Antenna for 360° Field of View

The five-port MIMO antenna is depicted in Fig. 1(b). The antenna is obtained by integrating a third patch and an isolation layer (RT5880 with $h_2 = 0.79$ mm) into the antenna to

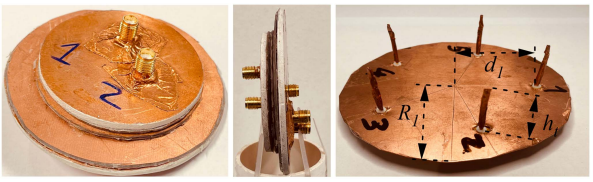

Fig. 2. Manufactured prototypes (not to scale). (a) Perspective-view; (b) side-view of the five-port multimode MIMO antenna; and (c) five-element circular array: $d_1 = 38\,\text{mm}$, $h_t = 28\,\text{mm}$, and $R_1 = 53\,\text{mm}$.

support TM_{31} modes. While this slightly increases the antenna size, the relatively small increase offers a significant improvement in performance, as will be demonstrated. The integrated patch is supported by a TMM6 substrate of thickness $h_4 = 2.54\,\text{mm}$, and using (1) $D_{31} = 73.8\,\text{mm}$. The patch is fed using P4 and P5 located at 16.5 mm from the disk center and oriented by $\alpha_2 = 30^\circ$, exciting two TM_{31} modes (see Table 1 columns 4 and 5). Because the integration of the new element influences the resonant frequencies of the other two, the antenna parameters were slightly tuned to compensate for this: the ground-plane of the middle patch ($D_{31} = 73.8\,\text{mm}$), s (15 mm), and a hole of radius $r_c = 5.25\,\text{mm}$ is drilled for P3 feeding. The total antenna size is then $73.8\,\text{mm} \times 73.8\,\text{mm} \times 8.45\,\text{mm}$ or $0.55\lambda \times 0.55\lambda \times 0.063\lambda$.

III. ANGLE OF ARRIVAL PERFORMANCE

The AoA performance is investigated using the MUSIC algorithm [15] implemented in MATLAB. The estimated AoA is extracted as the peak value of the MUSIC spectrum function, and the accuracy is evaluated in terms of mean absolute error (MAE) as

$$\phi_i^{\text{error}} = \frac{1}{M_{\text{MCr}}} \sum_{m=1}^{M_{\text{MCr}}} \left| \phi_i^{\text{MUSIC}} - \phi_i^{\text{incident}} \right| \tag{2}$$

where M_{MCr} is the number of Monte Carlo simulations performed for each angle ϕ_i, in this work $M_{\text{MCr}} = 800$ simulations. The incident angles (ϕ_i) are swept in the azimuth plane with 1° resolution.

Because the MUSIC algorithm assumes that the number of signals (K) is smaller than the number of elements/modes (N) in the antenna, i.e., $N > K$, a maximum of two simultaneous impinging signals can be separated in the three-port antenna, while a maximum of four simultaneous impinging signals can be identified with the five-port MIMO antenna.

Because the three-port MIMO antenna has a 180° FoV its performance is compared to a three-element linear array. In contrast, the five-port MIMO antenna achieves a 360° FoV, therefore, a five-element circular array is used for performance comparison. The traditional antenna array used as a reference consists of $\lambda/4$ monopole antennas, with the interspacing between elements chosen to provide the highest miniaturization that still ensures at least 10 dB isolation between antennas. Therefore, the final dimensions are $1.32\lambda \times 1.32\lambda \times 0.23\lambda$ and $0.85\lambda \times 0.85\lambda \times 0.25\lambda$ for three-element linear and five-element circular arrays, respectively. The proposed structures were manufactured and for brevity only the manufactured five-port MIMO antenna and five-element circular array are illustrated in Fig. 2. The anechoic chamber measurement setup is shown in Fig. 3(a), and the phase characteristics of the five-port MIMO are shown in Fig. 3(b). Despite some asymmetries due to phase reflections and the antenna holder during measurements, it is seen that the phase is nearly constant for the monopole (port 3) and changes linearly in opposing directions, twice for ports 1 and 2, and thrice for ports 4 and 5; following the

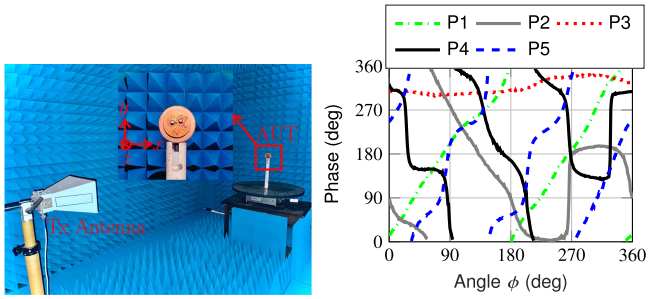

Fig. 3. Measured results. (a) Setup highlighting the antenna under test (AUT) and the transmitting (Tx) antenna. (b) Phase patterns of the AUT.

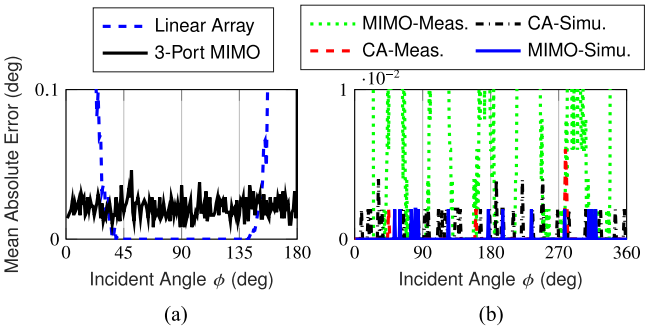

Fig. 4. Comparisons of the MUSIC performance for 12 dB SNR. (a) Three-port MIMO antenna and three-element linear array using 20 snapshots. (b) Five-port MIMO and five-element circular array using 200 snapshots.

required phase characteristics of the beamsteering principle outlined in Table 1. The isolation of the five-port MIMO is better than 17.6 dB in simulation and 11.6 dB in measurements. This discrepancy is attributed to manufacture and assembly tolerances, misalignment between the stacked layers, and the impact of the adhesive holding the layers. The ECC of the MIMO system is computed using the farfield patterns, as recommended in [17], and is below < 0.01 between all ports at $f_0 = 2.238\,\text{GHz}$.

A. Three-Port MIMO AoA Performance

Due to the AoA estimation ambiguity in linear arrays and three-port MIMO antenna, the AoA is constrained between $[0^\circ - 180^\circ]$ [18]. The performance is evaluated using (2) for 12 dB signal-to-noise ratio (SNR) and is shown in Fig. 4(a). It is seen that the FoV with MAE $< 0.05^\circ$ is 127° for the three-element linear array. The array MAE increases when approaching end-fire directions reaching values of up to 1.75°. In contrast, the performance of the three-port MIMO does not change with direction and it achieves a 180° FoV with MAE$< 0.05^\circ$. It should be noted that at broadside directions the linear array outperforms the three-port MIMO; however, the MIMO approach still offers low MAE and achieves such performance while using a structure of $0.4\lambda \times 0.4\lambda \times 0.037\lambda$; when compared to the linear array ($1.32\lambda \times 1.32\lambda \times 0.23\lambda$), this gives miniaturization of 70% in length and 84% in antenna height.

B. Five-Port MIMO AoA Performance

Fig. 4(b) shows the MUSIC performance of the five-port MIMO and five-element circular array. The results are computed using 200 snapshots and 12 dB SNR. It is observed that the array has MAE

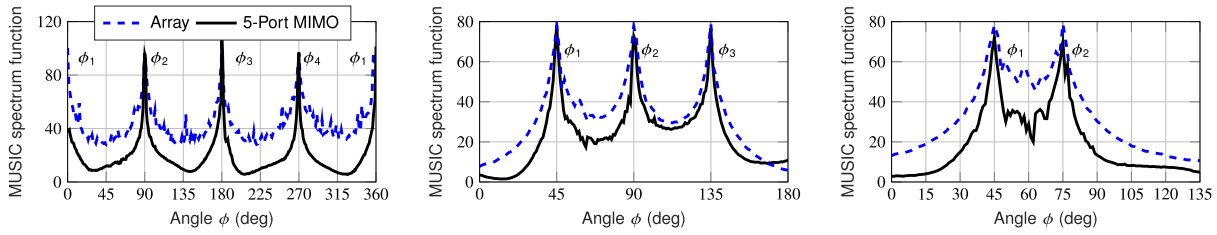

Fig. 5. Measured MUSIC spectrum (in dB) for five-port MIMO and five-element circular array. (a) Four simultaneous signals detection, where the directions are 90° apart covering the entire azimuth plane ($\phi_1 = 0/360°$, $\phi_2 = 90°$, $\phi_3 = 180°$, and $\phi_4 = 270°$). (b) Three signals detection for $\phi_1 = 45°$, $\phi_2 = 90°$, and $\phi_3 = 135°$. (c) Two signals detection for $\phi_1 = 45°$ and $\phi_2 = 75°$.

$< 0.008°$ in both the simulated and measured cases. The simulated five-port MIMO antenna shows peak MAE of 0.002°, changing to 0.098° in the measurements. Such discrepancies is most likely due to phase reflections during the measurements, which can contribute to increased AoA estimation errors; this is further highlighted in the phase characteristics [Fig. 3(b)], where the MAE peak regions have phase asymmetries and nonlinear behavior [around 40°–90° (port 4), 95° – 135° (port 5), 150° – 180° (port 5), 225°–260° (port 2), and 270° – 315° (ports 2 and 4)]. Note that this does not occur in the array due to the uniform phase pattern of the monopoles. Nevertheless, the realized AoA performance is still demonstrated with very low errors of up to 0.098° over the entire horizontal plane.

Fig. 5 shows the multiple signal separation for the MIMO and array designs. Fig. 5(a) demonstrates the proposed system capability to correctly detect four simultaneous arriving signals separated by 90°. It can be seen that the five-port MIMO leads to sharper peaks as compared to the circular array, with only four distinct peaks across the entire plane. The detection of three and two simultaneous signals using a smaller angular separation is shown in Fig. 5(b) and (c), respectively. Overall, both compared systems are capable to correctly detect the arriving signals; however, the MIMO shows sharper peaks in the MUSIC spectrum function. More importantly, as the MIMO requires only 0.55λ diameter, while the array occupies 0.85λ, a miniaturization of up to 35% is achieved when using the MIMO antenna, making the design suitable for miniaturized IoT devices.

IV. CONCLUSION

This work proposed the AoA estimation operating from a small platform, with performance comparable to larger state-of-the-art solutions while still using the same number of ports. It was demonstrated that the use of different orthogonal radiating modes within the same antenna volume allows for 360° field of view AoA estimations, with up to 35% size reduction compared to circular arrays and 70% compared to linear arrays. The achieved performance demonstrates the potential for multimode MIMO antennas as an enabling technology for IoT localization operating on compact devices. This is expected to find favorable applications in smart buildings, homes, and many other emerging IoT solutions.

ACKNOWLEDGMENT

This work was supported by the Science Foundation Ireland under Grant 18/SIRG/5612. The authors would like to thank Jakub Przepiorowski and Neeraj Maurya from Technological University Dublin for their help with antenna measurement and prototyping.

REFERENCES

[1] F. Zafari, A. Gkelias, and K. K. Leung, "A survey of indoor localization systems and technologies," *IEEE Commun. Surv. Tuts.*, vol. 21, no. 3, pp. 2568–2599, Jul.–Sep. 2019.

[2] D. Munoz, F. Bouchereau, C. Vargas, and R. Enriquez, *Position Location Techniques and Applications*. Burlington, MA, USA: Academic Press, 2009.

[3] T. E. Tuncer and B. Friedlander, *Classical and Modern Direction-of-Arrival Estimation*. Boston, MA, USA: Academic Press, 2009.

[4] A. M. Elbir, "Direction finding in the presence of direction-dependent mutual coupling," *IEEE Antennas Wireless Propag. Lett.*, vol. 16, no. 1, pp. 1541–1544, Jan. 2017.

[5] Z.-M. Liu, C. Zhang, and P. S. Yu, "Direction-of-arrival estimation based on deep neural networks with robustness to array imperfections," *IEEE Trans. Antennas Propag.*, vol. 66, no. 12, pp. 7315–7327, Dec. 2018.

[6] H.-S. Lui and H. T. Hui, "Direction-of-arrival estimation: Measurement using compact antenna arrays under the influence of mutual coupling," *IEEE Antennas Propag. Mag.*, vol. 57, no. 6, pp. 62–68, Dec. 2015.

[7] S. Kabiri, E. Kornaros, and F. De Flaviis, "Tightly coupled array design based on phase center contour for indoor direction findings in harsh environments," *IEEE Trans. Antennas Propag.*, vol. 68, no. 4, pp. 2698–2713, Apr. 2020.

[8] M. G. Pralon, G. Del Galdo, M. Landmann, M. A. Hein, and R. S. Thomä, "Suitability of compact antenna arrays for direction-of-arrival estimation," *IEEE Trans. Antennas Propag.*, vol. 65, no. 12, pp. 7244–7256, Dec. 2017.

[9] M. Burtowy, M. Rzymowski, and L. Kulas, "Low-profile ESPAR antenna for RSS-based DoA estimation in IoT applications," *IEEE Access*, vol. 7, pp. 17403–17411, 2019.

[10] S. Abielmona, H. V. Nguyen, and C. Caloz, "Analog direction of arrival estimation using an electronically-scanned CRLH leaky-wave antenna," *IEEE Trans. Antennas Propag.*, vol. 59, no. 4, pp. 1408–1412, Apr. 2011.

[11] M. Malajner, D. Gleich, and P. Planinšič, "Angle of arrival measurement using multiple static monopole atennas," *IEEE Sensors J.*, vol. 15, no. 6, pp. 3328–3337, Jun. 2015.

[12] C. Y. Kataria, G. X. Gao, and J. T. Bernhard, "Design of a compact hemispiral GPS antenna with direction finding capabilities," *IEEE Trans. Antennas Propag.*, vol. 67, no. 5, pp. 2878–2885, May 2019.

[13] R. Pöhlmann, S. A. Almasri, S. Zhang, T. Jost, A. Dammann, and P. A. Hoeher, "On the potential of multi-mode antennas for direction-of-arrival estimation," *IEEE Trans. Antennas Propag.*, vol. 67, no. 5, pp. 3374–3386, May 2019.

[14] L. Grundmann, N. Peitzmeier, and D. Manteuffel, "Investigation of direction of arrival estimation using characteristic modes," in *Proc. Eur. Conf. Antennas Propag.*, 2021, pp. 1–5.

[15] R. Schmidt, "Multiple emitter location and signal parameter estimation," *IEEE Trans. Antennas Propag.*, vol. 34, no. 3, pp. 276–280, Mar. 1986.

[16] R. Garg, P. Bhartia, B. I. Bahl, and A. Ittipboon, *Microstrip Antenna Design Handbook*. Norwood, MA, USA: Artech House, 2001.

[17] M. S. Sharawi, "Current misuses and future prospects for printed multiple-input, multiple-output antenna systems [Wireless Corner]," *IEEE Antennas Propag. Mag.*, vol. 59, no. 2, pp. 162–170, Apr. 2017.

[18] P. Ioannides and C. Balanis, "Uniform circular arrays for smart antennas," *IEEE Antennas Propag. Mag.*, vol. 47, no. 4, pp. 192–206, Aug. 2005.